J. Fluid Mech. (2016), *vol.* 809, R3, doi:10.1017/jfm.2016.725

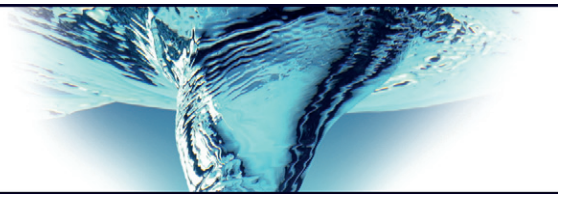

JFM RAPIDS
journals.cambridge.org/rapids

On the spreading of impacting drops under the influence of a vertical magnetic field

Jie Zhang[1,2], Tian-Yang Han[2], Juan-Cheng Yang[1,2] and Ming-Jiu Ni[2,†]

[1]State Key Laboratory for Strength and Vibration of Mechanical Structures, School of Aerospace, Xi'an Jiaotong University, Xi'an, Shaanxi 710049, China

[2]School of Engineering Science, University of Chinese Academy of Sciences, Beijing 101408, China

(Received 18 September 2016; revised 21 October 2016; accepted 30 October 2016; first published online 21 November 2016)

A theoretical model is developed to predict the maximum spreading of liquid metal drops when impacting onto dry surfaces under the influence of a vertical magnetic field. This model, which is constructed based on the energy conversion principle, agrees very well with the numerical results, covering a wide range of impact speeds, contact angles and magnetic strengths. When there is no magnetic field, we found that the maximum spreading factor can be predicted well by an interpolating scheme between the viscous and capillary effects, as proposed by Laan *et al.* (*Phys. Rev. Appl.*, vol. 2 (4), 2014, 044018). However, when gradually increasing the magnetic field strength, the induced Lorentz forces are dominant over the viscous and capillary forces, taking the spreading behaviour into the 'Joule regime', where the Joule dissipation is significant. For most situations of practical interest, namely when the strength of the magnetic field is less than 3 T, all three energy conversion routes are important. Therefore, we determine the correct scaling behaviours for the magnetic influence by first equating the loss of kinetic energy to the Joule dissipation in the Joule regime, then by interpolating it with the viscous dissipation and the capillary effects, which allows for a universal rescaling. By plotting the numerical results against the theoretical model, all the results can be rescaled onto a single curve regardless of the materials of the liquid metals or the contact angles of the surfaces, proving that our theoretical model is correct in predicting the maximum spreading factor by constructing a balanced formula between kinetic energy, capillary energy, viscous dissipation energy and Joule dissipation energy.

Key words: drops and bubbles, magnetohydrodynamics, materials processing flows

1. Introduction

Liquid drops impacting onto a solid surface present very important and fascinating phenomena, which are also of great importance in many practical processes, such as

† Email address for correspondence: mjni@ucas.ac.cn

inkjet printing and thermal spraying. In these applications, one of the most important dynamic behaviours is the maximum spreading of the drops, as shown by Yarin (2006). This impact behaviour is also key for liquid metal drops in the metallurgical industry and fusion engineering, where magnetic fields are always applied to control the flow of the liquid metal (Molokov & Reed 2000). In a fusion device, the divertor, which consists of a layer of liquid lithium, acts as a kind of plasma-facing component. Under a large heat flux, this liquid metal film will not be absolutely quiet and events like the formation of droplets, which would then impact on the dry surface, can occur. Therefore, the maximum spreading of liquid metal droplets under the influence of a magnetic field deserves more attention.

When there is no magnetic field, based on the balance between inertial and viscous and capillary contributions, numerous relations have been proposed to determine the maximum spreading factor, $\beta_{max} = D_{max}/D_0$, where D_{max} is the maximum spreading diameter and D_0 is the initial droplet diameter, as summarised by Josserand & Thoroddsen (2016). Although these models differ in their expressions, most of them are formulated using three impact parameters: the Weber number, $We = \rho D_0 V_0^2/\sigma$, standing for the ratio between the inertial and capillary force, the Reynolds number, $Re = \rho D_0 V_0/\mu$, describing the ratio between the inertial and the viscous force, and the contact angle θ, which depends on both the surface condition and dynamic behaviour. Here, ρ and μ are the density and dynamic viscosity of the liquid drop, respectively, σ is the surface tension, and V_0 is the impact velocity. In addition, when an external magnetic field is imposed, another dimensionless parameter, $N = \sigma_e B^2 D_0/\rho V_0$, needs to be considered, describing the ratio between the Lorentz force and the inertial force. Here, σ_e is the electrical conductivity and B is the magnetic field intensity.

By solving a detailed energy balance equation, a series of theoretical models have been established integrating the influence of We, Re and θ (Pasandideh-Fard *et al.* 1996; Roisman, Rioboo & Tropea 2002; Ukiwe & Kwok 2005; Lee *et al.* 2016). However, they are too complicated to be suitable for magnetohydrodynamics (MHD) problems, because we have to consider all four impact parameters (Re, We, N and θ) simultaneously during the spreading. Therefore, we turn to another approach, similar to that proposed by Laan *et al.* (2014).

Theory suggests that when the spreading of a droplet falls into the viscous regime, where viscous dissipation is dominant, a scaling of $\beta_{max} \propto Re^{1/5}$ is found by establishing energy conservation between the kinetic and the viscous dissipation energy (Clanet *et al.* 2004; Fedorchenko, Wang & Wang 2005). However, an alternative scaling of $\beta_{max} \propto Re^{1/4}$ was found by Pasandideh-Fard *et al.* (1996), who considered a drop becoming a pancake-shaped droplet at maximum spreading. Moreover, for the capillary regime, where viscous dissipation is negligible, the kinetic energy is almost entirely transferred into the surface energy and the maximum spreading factor obeys $\beta_{max} \propto We^{1/2}$, as found by Collings *et al.* (1990) and Bennett & Poulikakos (1993), or $\beta_{max} \propto We^{1/4}$, as found and verified by Clanet *et al.* (2004) and Tsai *et al.* (2011). Nevertheless, both Laan *et al.* (2014) and Eggers *et al.* (2010) found that the former expression of $\beta_{max} \propto We^{1/2}$ gave a better description of the spreading. Based on this, Laan *et al.* (2014) proposed a solution that introduced a broad cross-over regime between the viscous and capillary regimes by interpolating between $We^{1/2}$ and $Re^{1/5}$. By defining $P = We\,Re^{-2/5}$, the interpolated scheme is given as

$$\beta_{max} Re^{-1/5} \propto f_c(P), \quad \text{with } f_c(P) = P^{1/2}/(A + P^{1/2}), \tag{1.1}$$

where A is a constant. This interpolated relation between the two scaling laws showed good agreement with experimental data. However, Laan's approach did not consider the wettability of the drop on the surface, and this model was further improved recently by Lee *et al.* (2015).

Following the method of Laan *et al.* (2014), when an external vertical magnetic field is imposed, we first obtain a relation between β_{max} and N in the Joule regime, in which almost all the kinetic energy is transferred into Joule dissipation. In this way, we suppose $\beta_{max} \propto N^{\alpha}$, where α is the power exponent. After that, we establish a theoretical model to predict the maximum spreading factor by interpolating between $We^{1/2}$, $Re^{1/5}$ and N^{α}. In addition, we should also consider the influence of wettability of the dry surface.

As far as the authors know, although the spreading behaviour of liquid metal drops under the influence of a magnetic field is important in the metallurgical industry and fusion engineering, no available references have been published until now. The most similar studies are those of liquid metal droplets impacting onto a thin liquid film under the influence of a magnetic field (Wang *et al.* 2014; Tagawa 2005), which can provide some reference results for us. In the present study, we use direct numerical simulations to obtain adequate results with different liquid metals, different impact velocities, different magnetic strengths and different static contact angles. Then, we compare the scaling law we propose with the numerical results, in order to validate its correctness. It should be noted that we will not consider the effect of splash, rim instability or the influence of the surrounding gas; we also assume that the liquid metal drop will not solidify on the solid surface and its physical properties are constant. Therefore, when the magnetic field is applied along the impact direction, the three-dimensional problem can be solved using two-dimensional cylindrical coordinates.

2. Physical model and numerical methods

Let us consider a spherical droplet of liquid metal impacting onto a dry surface with a falling velocity V_0, which can vary from 0.6 to 6 m s^{-1}, and an applied vertical magnetic field B_z, which can vary from 0 to 6 T. It should be noted that this parameter space is much wider than that used in the metallurgic industry and fusion devices, where B is always smaller than 3 T. The spreading problem is sketched in figure 1, where $-r$ and $-z$ are the radial and impacting directions. Also, different kinds of liquid metals are used for the numerical simulations: specifically, liquid GaInSn, liquid lithium and liquid mercury, whose physical properties are given in table 1. If we fix the drop diameter at $D_0 = 2$ mm, the impact parameters can be expected to fall into the ranges $We = 20 \sim 100$, $Re = 6 \times 10^3 \sim 1.8 \times 10^4$ and $N = 0 \sim 16$, which can provide enough data for our analysis. Moreover, when the liquid drop spreads over the solid surface, the contact angle θ is also an important factor to determine the spreading behaviour; therefore, we choose three values of 60°, 90° and 120° in the present study to represent a range of hydrophilic and hydrophobic surfaces. It should be noted that, in practical applications, the contact angle varies dynamically with the speed of advance or recession of the free surface; however, to make things simpler, we use a static contact angle throughout the paper. Consequently, more than three hundred numerical simulations will be carried out in the following study in order to render a more comprehensive conclusion.

By using D_0, V_0, ρV_0^2 and $\sigma_e V_0 B_z$ as typical scales for the length, velocities, pressure and electric current densities, respectively, the axisymmetric and dimensionless

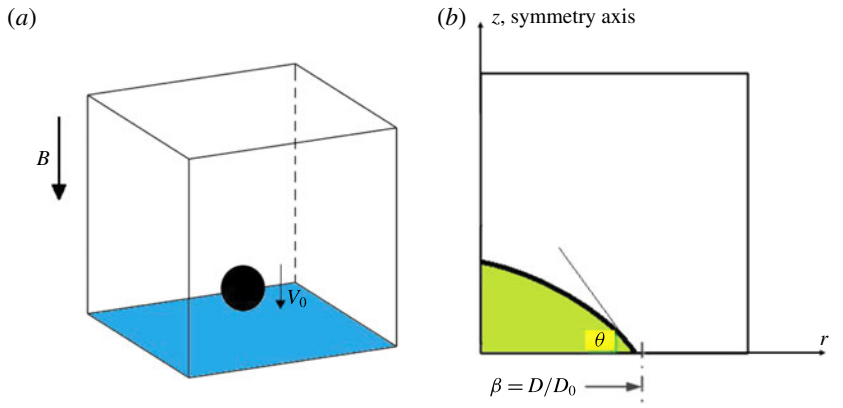

FIGURE 1. Sketches of (*a*) the physical model at the initial moment and (*b*) the spreading of the drop with contact angle.

Liquid	ρ (kg m^{-3})	μ (Pa s)	σ (N m^{-1})	σ_e (1Ω^{-1} m^{-1})
GaInSn	6361	2.2×10^{-3}	0.553	3.27×10^{6}
Lithium	515	5.716×10^{-4}	0.39	3.626×10^{6}
Mercury	13 610	1.53×10^{-3}	0.46	1.0×10^{6}

TABLE 1. Properties of the liquids used in the numerical simulations.

continuity and Navier–Stokes equations controlling the spreading problem in cylindrical coordinates become:

$$\frac{1}{r}\frac{\partial}{\partial r}(rV_r) + \frac{\partial V_z}{\partial z} = 0, \tag{2.1}$$

$$\frac{\partial V_r}{\partial t} + V_r\frac{\partial V_r}{\partial r} + V_z\frac{\partial V_r}{\partial z} - \frac{V_\theta^2}{r} = -\frac{\partial p}{\partial r} + \frac{1}{Re}\left(\Delta V_r - \frac{V_r}{r^2}\right) + \frac{\kappa}{We}\frac{\partial c}{\partial r} - NV_r, \tag{2.2}$$

$$\frac{\partial V_\theta}{\partial t} + V_r\frac{\partial V_\theta}{\partial r} + V_z\frac{\partial V_\theta}{\partial z} + \frac{V_\theta V_r}{r} = \frac{1}{Re}\left(\Delta V_\theta - \frac{V_\theta}{r^2}\right) + N\left(\frac{\partial \varphi}{\partial r} - V_\theta\right), \tag{2.3}$$

$$\frac{\partial V_z}{\partial t} + V_r\frac{\partial V_z}{\partial r} + V_z\frac{\partial V_z}{\partial z} = -\frac{\partial p}{\partial z} + \frac{1}{Re}(\Delta V_z) + \frac{\kappa}{We}\frac{\partial c}{\partial z}, \tag{2.4}$$

where Δ is the Laplace operator, defined as $\Delta V = (\partial^2 V/\partial r^2) + (1/r)(\partial V/\partial r) + (\partial^2 V/\partial z^2)$ in cylindrical coordinates, and c is the fraction of the liquid phase for the surface tension calculation within a continuum approach developed by Brackbill, Kothe & Zemach (1992). Here, φ is the induced electric potential, which is scaled by $V_0 D_0 B_z$ and calculated by solving a Poisson equation:

$$\Delta\varphi = \frac{V_\theta}{r} + \frac{\partial V_\theta}{\partial r}. \tag{2.5}$$

Because V_θ, the circumferential velocity, is supposed to be zero in our previous hypothesis, therefore (2.3) and (2.5) are eliminated. Correspondingly, the Lorentz force, which also vanishes in the circumferential direction, exists only in the radial direction, acting counter to the spreading motion, as shown in (2.2).

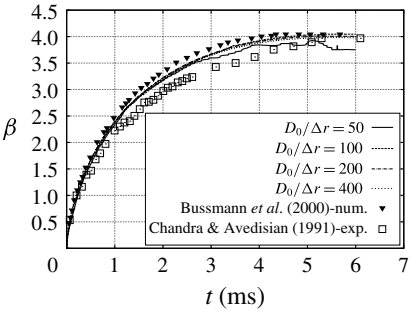

FIGURE 2. The convergence study of the spatial resolution, with impact parameters $Re = 2300$, $We = 43$ and $\theta = 32°$. It is observed that all results agree very well with the numerical solutions by Bussmann *et al.* (2000) except the case with a spatial resolution of $D_0/\Delta r = 50$.

For the numerical approach, we use the open source volume-of-fluid solver Gerris (Popinet 2009) to simulate the impact event. Gerris solves the incompressible Navier-Stokes equation within an adaptive mesh framework, and the interface capturing and reconstructing schemes are physically sound and accurate, rendering it very appropriate for simulating multiphase flows. With the help of Gerris, there are some papers that study the drop impact problem (Thoraval *et al.* 2012; Agbaglah *et al.* 2015; Wildeman *et al.* 2016), presenting very promising results.

In each simulation the axisymmtric drop was set in a domain with a width of $L = 10D_0$, which is large enough for the drop to spread because the value of We is not high ($We < 100$). Furthermore, in order to study the convergence of the grids, we compute a test case with different spatial resolutions, namely $D_0/\Delta r = 50$, 100, 200, 400, respectively, where Δr is the minimum mesh size inside the drop. The test case has also been studied by Bussmann, Chandra & Mostaghimi (2000), with impact parameters of $Re = 2300$, $We = 43$ and $\theta = 32°$, and the comparisons between our results and those of Bussmann are plotted in figure 2, where the squares are the experimental results given by Chandra & Avedisian (1991). As presented, all the results are in good agreement with those of Bussmann, except the case solved with $D_0/\Delta r = 50$; however, deviations are observed from the experimental data, and should be ascribed to the dynamic contact angle in the experiment. Therefore, for consideration of computational efficiency and accuracy, we will select $D_0/\Delta r = 200$ across the drop as the spatial discretisation.

3. Results

3.1. *Spreading behaviour without a magnetic field*

Without a magnetic field, as introduced in § 1, the interpolating scheme of (1.1) can be used to predict β_{max} in the cross-over regime where viscous and capillary forces are both important. As a consequence, part of our numerical results, which are conducted with fixed $\theta = 90°$ and different liquid metals, are plotted in figure 3 to verify whether this interpolating scheme is applicable. In figure 3(*a*), all the data are observed to fall onto a single curve with the scaling law interpolated between $Re^{1/5}$ and $We^{1/2}$, which is fitted accurately with (1.1). However, in figure 3(*b*), the interpolating law between $Re^{1/5}$ and $We^{1/4}$ does not collapse the data points onto a single curve – as was also found by Eggers *et al.* (2010).

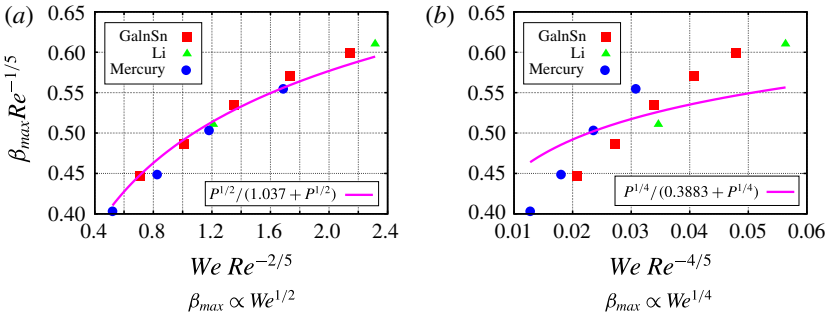

FIGURE 3. The maximum spreading factor rescaled by different interpolating scheme when $\theta = 90°$. (*a*) As a function of $We\,Re^{-2/5}$. (*b*) As a function of $We\,Re^{-4/5}$. The solid line is the Padé approximant function fitted with (1.1). It is observed that all data fall onto a single curve fitted with the scaling law of $\beta_{max} \propto Re^{1/5} f_c(We\,Re^{-2/5})$, while contrary results are found in the scaling law of $\beta_{max} \propto Re^{1/5} f_c(We\,Re^{-4/5})$.

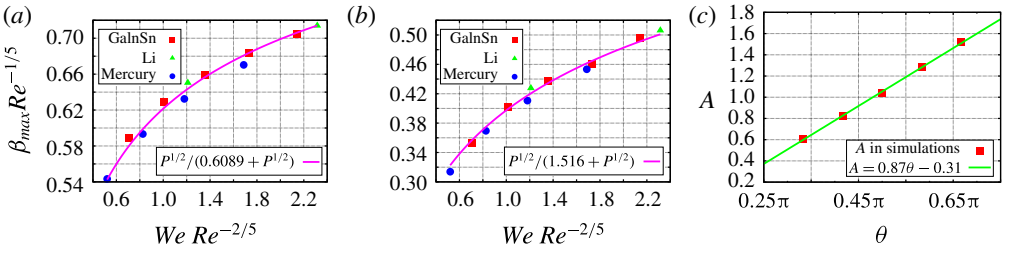

FIGURE 4. The maximum spreading factor rescaled with a function of parameter $We\,Re^{-2/5}$ for various contact angles: (*a*) $\theta = 60°$, (*b*) $\theta = 120°$. It is found that they conform to the same scaling law of (1.1), although the constant coefficient A is different. (*c*) The variation trend of A with different surface wettability, showing that A increases almost linearly with θ.

However, equation (1.1) does not consider the influence of surface wettability. We have further investigated this by changing the contact angle to $\theta = 60°$ and $\theta = 120°$, and the results are shown in figure 4(*a*,*b*). It is observed that all results still obey the scaling law of (1.1); however, the fitting constant A is different, indicating that A is determined by the surface wettability. To investigate this further, we simulate additional numerical cases with $\theta = 75°$ and $\theta = 105°$ to determine the correction between A and θ; the result is presented in figure 4(*c*), where a linear relation is observed between them.

3.2. *Spreading behaviour under a vertical magnetic field*

When a vertical magnetic field is applied, the induced Lorentz force, which acts as a resistance to the spreading, will decrease the maximum spreading radius. The evolution of the droplet shapes of liquid GaInSn during spreading is presented in figure 5, respectively without and with magnetic field, with other fixed parameters of $Re = 13\,422$, $We = 96$ and $\theta = 90°$. It is observed that, with $N = 0$, the spreading factor gradually increases to $\beta_{max} \approx 4$ while the height of the droplet keeps decreasing. In contrast, in the case of $N = 5.660$, the maximum spreading factor decreases to

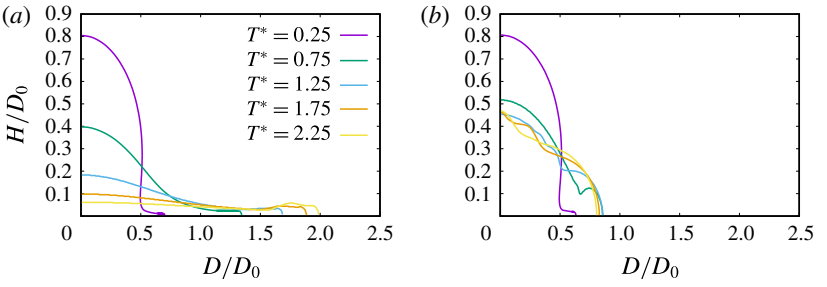

FIGURE 5. The evolution of the droplet shapes during the spreading process without and with magnetic field respectively, with other fixed parameters of $Re = 13\,422$, $We = 96$ and $\theta = 90°$. (*a*) $N = 0$, (*b*) $N = 5.660$. It is observed that β_{max} decreases significantly under the influence of a magnetic field; moreover, the interface of the droplet fluctuates after attaining the maximum spreading radius.

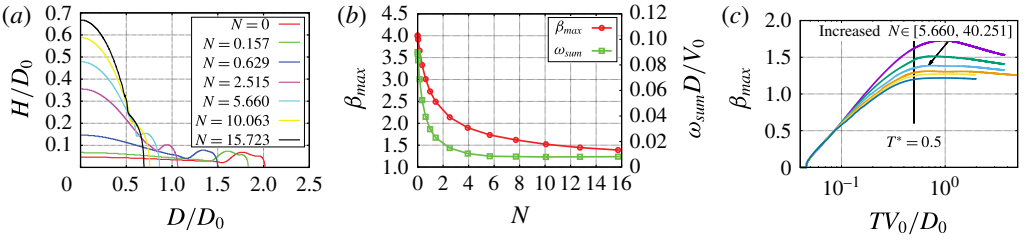

FIGURE 6. Spreading behaviours under the influence of different vertical magnetic fields, the working medium is GaInSn and the fixed parameters are $Re = 13\,422$, $We = 96$ and $\theta = 90°$, while the magnetic intensity is varied from $N = 0$ to $N = 16$ for (*a*,*b*) or from $N = 5.66$ to $N = 40.251$ for (*c*). (*a*) The shape of the drop interface when the maximum spreading radius occurs. (*b*) The variation of the maximum spreading factor β_{max} and the sum of the vorticities inside the drop at that moment. (*c*) The time histories of the spreading with a strong magnetic field, for which it is found that t_m converges to $D_0/2V_0$ when N is much larger.

$\beta_{max} \approx 1.7$; thereafter, the interface of the droplet starts to fluctuate while the spreading radius remains almost unchanged.

The droplet shapes, at the moment when β_{max} occurs, are plotted against N in figure 6(*a*), as the magnetic intensity is varied from $N = 0$ to $N = 16$. In the figure, the maximum spreading radius is restrained by stronger magnetic fields; the rim region, which bulges out of the spreading drop, is also narrowed. It is well known that there are recirculation eddies formed in the rim, even if the drop stops moving at maximum spreading radius. The maximum spreading radius, as well as the sum of the vorticities inside the drop at that moment, is shown in figure 6(*b*). It is observed that the spreading radius is dramatically reduced by the magnetic field within the range of smaller N; however, the reducing trend slows when N becomes larger. That is because, under such a stronger magnetic field, the spreading velocity will be much slower, and the Lorentz force, whose value has a necessary limit based on the inertia, will also decrease to maintain this force balance. This variation trend is very similar to that found in the rising of bubbles (Zhang, Ni & Moreau 2016). Meanwhile, the evolution of ω_{sum} at that moment obeys a similar law, indicating that vortices are greatly suppressed by the Lorentz force. In figure 6(*c*), we also plot the time histories

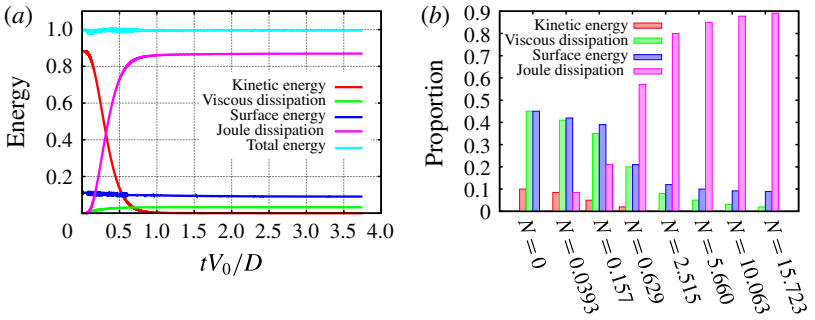

FIGURE 7. The influence of vertical magnetic field on different components of energy consumption; the fixed impact parameters are $Re = 13\,422$, $We = 96$ and $\theta = 90°$. (*a*) Evolutions of different energies with $N = 10.063$. (*b*) The final proportions of different energies with various values of N.

of the spreading under stronger magnetic field ($5.660 < N < 40.251$), in order to track the time when maximum spreading is reached, defined as t_m. In the figure, it is observed that, with stronger magnetic field, t_m gradually converges to $t_m = D_0/2V_0$; the detailed physics of this time scale will be presented in § 3.3.

Furthermore, to study in-depth the influence of a magnetic field on the spreading behaviour, the energy conversion process during spreading should be investigated. Under a strong magnetic field, as a result of the Joule dissipation, the initial kinetic energy will be dissipated in a very short time. Considering that the gravitational potential energy is negligible during the spreading, the energy conservation equation can be written as

$$KE_0 + SE_0 = KE + VE + SE + JE, \tag{3.1}$$

where KE is the kinetic energy, VE is the viscous dissipation energy and SE is the surface energy – the expressions for which can be found in many papers (Bennett & Poulikakos 1993; Pasandideh-Fard *et al.* 1996). The subscript 0 indicates the initial energy before impact. Under an external magnetic field, JE is the Joule dissipation, taking the form

$$JE = \int_0^t \int_V \boldsymbol{V}(r, z) \cdot (\boldsymbol{j}(r, z) \times \boldsymbol{B})\, \mathrm{d}V\, \mathrm{d}t, \tag{3.2}$$

where $\boldsymbol{j}$ is the induced electric current, given as $\boldsymbol{j} = \sigma_e \boldsymbol{V} \times \boldsymbol{B}$.

In particular, considering a test case of $N = 10.063$, the time histories of different components of the energy are presented in figure 7(*a*). As shown in the figure, the kinetic energy is dissipated rapidly once the impact starts. During the spreading process, almost all the initial kinetic energy is transferred into Joule dissipation, which ultimately takes 87 % of the total energy. In contrast, the viscous dissipation effect and capillary effect are negligible throughout the spreading. To study the influence of the magnetic strength on energy conversion, the final proportions of different energy components versus N have been plotted at the time when the maximum spreading radius is reached, as shown in figure 7(*b*). It is observed that, with stronger magnetic field, the proportion of Joule dissipation increases correspondingly, while the other energies decrease monotonously. Therefore, besides the viscous regime and capillary

regime in which the viscous force and capillary force dominate respectively, we have another 'Joule regime', in which the Joule dissipation is dominant over the other two effects, such as for $N > 2.515$ in figure 7(*b*).

Consequently, we are able to interpret why β_{max} becomes smaller with larger N – because more kinetic energy is dissipated by Joule dissipation, hardly any residual energy is left for the drop to spread on the surface.

3.3. *Scaling law for predicting the maximum spreading factor*

To derive the maximal spreading radius under the combination of the viscous, capillary and Joule effects, according to our routine outline described in § 1, we will first consider the extreme Joule regime in which the kinetic energy is completely dissipated by Joule dissipation. Under such circumstances, the initial kinetic energy is estimated as:

$$KE_0 \sim \rho V_0^2 D_0^3. \tag{3.3}$$

According to (3.2), when the drop is at its maximum extension, Joule dissipation is calculated as

$$JE = \int_0^t \int_V \boldsymbol{V}(r, z) \cdot (\boldsymbol{j}(r, z) \times \boldsymbol{B}) \, \mathrm{d}V \, \mathrm{d}t = \sigma_e \overline{V_r}^2 B_z^2 \Omega t_m, \tag{3.4}$$

where Ω is the drop volume, scaling as $\Omega \sim D_0^3$, leaving the scale of t_m to be considered further. For hydrodynamic spreading of the droplet, Eggers *et al.* (2010) and Josserand & Zaleski (2003) have proved theoretically that in the very first stage of the impact, the pressure at the centre of the impact is very high, and this strong pressure gradient drives the liquid to spread. In this pressure-driven stage, the time scale is $t \sim D_0/2V_0$. After that, the pressure decreases rapidly and the fluid flow becomes similar to a time-dependent hyperbolic flow, in which the viscous effect and capillary effect gradually increase until maximum spreading is reached.

When imposing the magnetic field, the first pressure-driven stage should still keep a time scale of $t \sim D_0/2V_0$ because the pressure gradient is very strong and the Lorentz force, which is dependent on the spreading velocity, is still increasing. However, in the second stage, with a rapidly decaying pressure, the inertial force of the liquid is almost balanced by the Lorentz force, and the spreading decelerates according to

$$\frac{\mathrm{D}V_r}{\mathrm{D}t} = -\frac{1}{\rho}(\boldsymbol{j} \times \boldsymbol{B}) \cdot \boldsymbol{e}_r = -(\sigma_e B_z^2/\rho) V_r, \tag{3.5}$$

where $\boldsymbol{e}_r$ is the radial direction vector. Clearly, the Lorentz force acts on a time scale of

$$\tau = \rho/(\sigma_e B_z^2). \tag{3.6}$$

We now compare the time scale with the characteristic time of $T_0 = D_0/V_0$, that is

$$\frac{\tau}{T_0} = \frac{\rho V_0}{\sigma_e B_z^2 D_0} = \frac{1}{N}. \tag{3.7}$$

In the Joule regime, where N is much larger, it is easy to deduce $\tau/T_0 \ll 1$. It means the kinetic energy will be dissipated by the Joule effect within a very short time after the pressure drops. Under such circumstances, the time is ignored in this

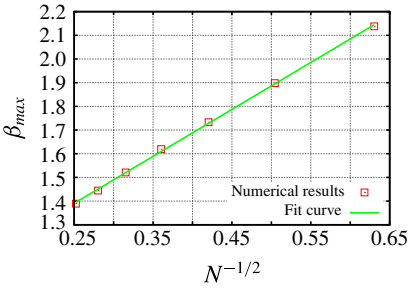

FIGURE 8. A test of the scaling law of (3.8) in the Joule regime, using β_{max} calculated from our numerical simulations within fixed $Re = 13\,422$, $We = 96$, $\theta = 90°$ and varied N from 2.515–15.723. It is observed that all results collapse onto a single curve fitting with $\beta_{max} \sim N^{-1/2}$, indicating that (3.8) is totally applicable in the Joule regime.

stage. Therefore, t_m will converge to the first stage, given as $t_m \sim D_0/2V_0$. This is also validated in our numerical simulations, as described previously in figure 6(*c*).

Therefore, the average radial velocity scales as $\overline{V_r} \sim D_{max}V_0/D_0$. Taking all of them into (3.4), and supposing $KE_0 = JE$, by which the kinetic energy is balanced by the Joule dissipation, we finally obtain

$$\rho V_0^2 D_0^3 \sim \sigma_e D_{max}^2 D_0^2 B_z^2 V_0 \Rightarrow \beta_{max} = \frac{D_{max}}{D_0} \sim N^{-1/2}. \tag{3.8}$$

To validate the correctness of this scaling law in the Joule regime, we present the evolution of β_{max} from our numerical results with $Re = 13\,422$, $We = 96$, $\theta = 90°$ and $N > 2.515$, and plot the comparative results in figure 8. We observe that the numerical results are predicted accurately by the scaling law (3.8), which shows a positive correction between β_{max} and $N^{-1/2}$ in the Joule regime.

After obtaining $\beta_{max} \propto N^{-1/2}$ in the Joule regime, we should consider a more general situation in which all the viscous, capillary and Joule effects can be condensed into one scaling relation depending on the group of variables $\{Re^{1/5}, We^{1/2}, N^{-1/2}, \theta\}$. Although (1.1) is proved to be effective by constructing an interpolating scheme in the cross-over regime between the viscous and capillary regimes, it will be much more difficult to put $N^{-1/2}$ in, because there will be three variables contained in the interpolation function. Moreover, if the contact angle is also taken into consideration for a more universal scaling law, things will become even more complex.

Alternatively, we can define a new variable, β_0, which represents the maximal spreading factor without magnetic field, namely under $N = 0$. In this way, the viscosity effect, the capillary effect and the influence of wettability are all integrated into β_0, which can be calculated by (1.1). Consequently, the problem of constructing an interpolation scheme is simplified into interpolating between β_0 and $N^{-1/2}$ scaling. To test this possibility, we adopt an approach similar to Eggers *et al.* (2010) and Laan *et al.* (2014) by constructing a function

$$\beta_{max} \propto N^{-1/2} f_c(\beta_0^2 N), \tag{3.9}$$

where f_c is a function of the parameter $\beta_0^2 N$; we also introduce the impact parameter $L = \beta_0^2 N$ to identify the relative influence between the three effects. According to this function, we plot all numerical results obtained with $\theta = 90°$, as shown in figure 9(*a*).

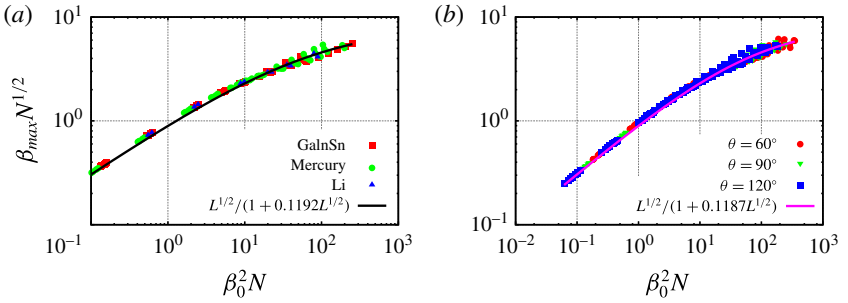

FIGURE 9. The rescaled maximum spreading ratio as a function of β_0^2N, with the solid line showing the interpolating function (3.10) fitted to the numerical results. (*a*) The numerical results obtained within fixed θ of 90° when using different liquid metals as working medium. (*b*) The numerical results obtained within different θ of 60°, 90° and 120°. It is observed that no matter what liquid metal we use, and no matter what contact angle we set, all results collapse onto the single curve given by (3.10).

From the figure, we observe this approach indeed succeeds in collapsing all data points for different liquid metals and impact velocities onto a single curve. It indicates that (3.9) is applicable in describing the maximum spreading radius in the cross-over regime between the viscous, capillary and Joule regimes.

To make (3.9) more quantitative, we also adopt the Padé approximant by constructing the formulation of $f_c(L)$, equation (3.9) is transformed to

$$\beta_{max}N^{1/2} = L^{1/2}/(1 + BL^{1/2}), \quad L = \beta_0^2N, \tag{3.10}$$

where B is the fitting constant, and $f_c(L)$ satisfies $\lim_{L\to 0}\beta_{max} = \beta_0$, $\lim_{L\to\infty}\beta_{max} \propto N^{-1/2}$.

The fit of (3.10) agrees excellently with the numerical results, as shown in figure 9(*a*), where the determination coefficient R^2 is 0.988, indicating that (3.10) is very effective in predicting the maximum spreading radius in the cross-over regime.

Moreover, as we stated, the influence of θ is included in β_0, so (3.10) should be applicable for different contact angles. To validate this, all numerical results, calculated with $\theta = 60°$, $\theta = 90°$ and $\theta = 120°$ respectively, are plotted in figure 9(*b*) with the formulation of (3.9). From the figure, it is observed that all the data are collapsed onto a single curve, which can be fitted well by the scaling law of (3.10). Therefore, the analytical solution, which is based on the energy conservation principle, describes the spreading behaviour very well with various liquids, impact velocities, external magnetic fields and contact angles.

Regarding the influence of a dynamic contact angle θ_d in practical droplet spreading problems, we think it can be divided into two aspects: (i) The influence of θ_d on β_0. According to Pasandideh-Fard *et al.* (1996), it is less accurate to predict β_{max} by using a constant equilibrium contact angle instead of using θ_d. However, this discrepancy between the two results will be very limited when the two contact angles are close. Also, Laan *et al.* (2014) have proved that (1.1) fits very well with the experimental results, where the contact angle is definitely dynamic. (ii) The influence of θ_d on $N^{-1/2}$. As presented in the derivation of (3.8), t_m is almost dependent on the first pressure-driven stage, in which the influence of θ_d is also limited. Therefore, our model should be applicable in practical situations even if the contact angle is dynamic.

4. Conclusion

In summary, we show that a universal analytical solution can be used to describe the maximum spreading of fluids when an external vertical magnetic field is imposed. This scaling law can deal with the cross-over regime between the viscous, capillary and Joule regimes, which covers most of the practical situations in the metallurgical industry or fusion devices. To obtain this scaling relation, we take three steps: first, with our numerical results, we verify the correctness of the solution given by Laan *et al.* (2014), who developed an interpolating scheme between viscous and capillary regimes without a magnetic field, scaling as $\beta_{max} \propto Re^{1/5}$ and $\beta_{max} \propto We^{1/2}$; second, by conserving the balance between kinetic energy and Joule dissipation when Joule dissipation is dominant over the viscous and capillary effects, we derive a relation between β_{max} and N, scaling as $\beta_{max} \propto N^{-1/2}$; finally, we construct an interpolating scheme integrating the influence of the viscous, capillary and Joule effects, which can be expressed by a group of variables $\{Re^{1/5}, We^{1/2}, N^{-1/2}, \theta\}$. However, to make things clearer and more direct, we define a new impact parameter β_0 to describe the maximum spreading factor without a magnetic field. Subsequently, only two impact parameters are considered in our model, with which we give a scaling law of $\beta_{max} \propto N^{-1/2} f_c(\beta_0^2 N)$.

Furthermore, the accuracy and validity of the scaling law is validated by fitting it with our numerical results, and very good agreement is observed between them regardless of the impact conditions and magnetic intensities. The comparison shows that the analytic relation can be approximated with an Padé approximant, scaling as $\beta_{max} N^{1/2} = L^{1/2}/(1 + BL^{1/2})$. More generally, the results of this study may be used over a wide range of applications in industry and fusion engineering, for which the control of drop impacting under the influence of a magnetic field is of great importance.

Acknowledgement

This work has been supported by NSFC (nos. 51636009, 11502193) and by MOST (no. 2013GB114000).

References

AGBAGLAH, G., THORAVAL, M.-J., THORODDSEN, S., ZHANG, L., FEZZAA, K. & DEEGAN, R. 2015 Drop impact into a deep pool: vortex shedding and jet formation. *J. Fluid Mech.* **764**, R1.

BENNETT, T. & POULIKAKOS, D. 1993 Splat-quench solidification: estimating the maximum spreading of a droplet impacting a solid surface. *J. Mater. Sci.* **28** (4), 963–970.

BRACKBILL, J., KOTHE, D. B. & ZEMACH, C. 1992 A continuum method for modeling surface tension. *J. Comput. Phys.* **100** (2), 335–354.

BUSSMANN, M., CHANDRA, S. & MOSTAGHIMI, J. 2000 Modeling the splash of a droplet impacting a solid surface. *Phys. Fluids* **12** (12), 3121–3132.

CHANDRA, S. & AVEDISIAN, C. 1991 On the collision of a droplet with a solid surface. *Proc. R. Soc. Lond.* A **432**, 13–41.

CLANET, C., BÉGUIN, C., RICHARD, D. & QUÉRÉ, D. 2004 Maximal deformation of an impacting drop. *J. Fluid Mech.* **517**, 199–208.

COLLINGS, E., MARKWORTH, A., MCCOY, J. & SAUNDERS, J. 1990 Splat-quench solidification of freely falling liquid-metal drops by impact on a planar substrate. *J. Mater. Sci.* **25** (8), 3677–3682.

EGGERS, J., FONTELOS, M., JOSSERAND, C. & ZALESKI, S. 2010 Drop dynamics after impact on a solid wall: theory and simulations. *Phys. Fluids* **22** (6), 062101.

FEDORCHENKO, A., WANG, A.-B. & WANG, Y.-H. 2005 Effect of capillary and viscous forces on spreading of a liquid drop impinging on a solid surface. *Phys. Fluids* **17** (9), 093104.

JOSSERAND, C. & THORODDSEN, S. 2016 Drop impact on a solid surface. *Annu. Rev. Fluid Mech.* **48**, 365–391.

JOSSERAND, C. & ZALESKI, S. 2003 Droplet splashing on a thin liquid film. *Phys. Fluids* **15** (6), 1650–1657.

LAAN, N., DE BRUIN, K., BARTOLO, D., JOSSERAND, C. & BONN, D. 2014 Maximum diameter of impacting liquid droplets. *Phys. Rev. Appl.* **2** (4), 044018.

LEE, J., DEROME, D., GUYER, R. & CARMELIET, J. 2016 Modeling the maximum spreading of liquid droplets impacting wetting and nonwetting surfaces. *Langmuir* **32** (5), 1299–1308.

LEE, J., LAAN, N., DE BRUIN, K., SKANTZARIS, G., SHAHIDZADEH, N., DEROME, D., CARMELIET, J. & BONN, D. 2015 Universal rescaling of drop impact on smooth and rough surfaces. *J. Fluid Mech.* **786**, R4.

MOLOKOV, S. & REED, C. 2000 Review of free-surface mhd experiments and modeling. *Tech. Rep.* Argonne National Lab., IL (US).

PASANDIDEH-FARD, M., QIAO, Y., CHANDRA, S. & MOSTAGHIMI, J. 1996 Capillary effects during droplet impact on a solid surface. *Phys. Fluids* **8** (3), 650–659.

POPINET, S. 2009 An accurate adaptive solver for surface-tension-driven interfacial flows. *J. Comput. Phys.* **228** (16), 5838–5866.

ROISMAN, I., RIOBOO, R. & TROPEA, C. 2002 Normal impact of a liquid drop on a dry surface: model for spreading and receding. *Proc. R. Soc. Lond.* A **458**, 1411–1430.

TAGAWA, T. 2005 Numerical simulation of a falling droplet of liquid metal into a liquid layer in the presence of a uniform vertical magnetic field. *ISIJ Int.* **45** (7), 954–961.

THORAVAL, M.-J., TAKEHARA, K., ETOH, T., POPINET, S., RAY, P., JOSSERAND, C., ZALESKI, S. & THORODDSEN, S. 2012 von kármán vortex street within an impacting drop. *Phys. Rev. Lett.* **108** (26), 264506.

TSAI, P., HENDRIX, M., DIJKSTRA, R., SHUI, L. & LOHSE, D. 2011 Microscopic structure influencing macroscopic splash at high weber number. *Soft Matt.* **7** (24), 11325–11333.

UKIWE, C. & KWOK, D. 2005 On the maximum spreading diameter of impacting droplets on well-prepared solid surfaces. *Langmuir* **21** (2), 666–673.

WANG, J.-J., ZHANG, J., NI, M.-J. & MOREAU, R. 2014 Numerical study of single droplet impact onto liquid metal film under a uniform magnetic field. *Phys. Fluids* **26** (12), 122107.

WILDEMAN, S., VISSER, C., SUN, C. & LOHSE, D. 2016 On the spreading of impacting drops. *J. Fluid Mech.* **805**, 636–655.

YARIN, A. 2006 Drop impact dynamics: splashing, spreading, receding, bouncing. *Annu. Rev. Fluid Mech.* **38**, 159–192.

ZHANG, J., NI, M.-J. & MOREAU, R. 2016 Rising motion of a single bubble through a liquid metal in the presence of a horizontal magnetic field. *Phys. Fluids* **28** (3), 032101.